JCTC Journal of Chemical Theory and Computation

Article

pubs.acs.org/JCTC

Cooperative Contributions of the Intermolecular Charge Fluxes and Intramolecular Polarizations in the Far-Infrared Spectral Intensities of Liquid Water

Hajime Torii*

Department of Chemistry, School of Education, Shizuoka University, 836 Ohya, Shizuoka 422-8529, Japan

ABSTRACT: The main factors that determine the infrared and far-infrared (terahertz) spectral features of liquid water in the frequency region below 1000 cm^{-1} are examined theoretically. By analyzing the modulations of electron populations induced by molecular translations in water clusters, it is shown that there is an approximate linear relation between the derivative of intermolecular electron population transfer ($\partial\rho_{D\leftarrow A}/\partial r_{O\cdots H}$) and the hydrogen-bond length ($r_{O\cdots H}$). This relation is used to incorporate the effects of hydrogen-bond fluctuations and defects into the intensity generation mechanisms in the spectral simulations of liquid water based on classical molecular dynamics, showing that intermolecular charge fluxes and intramolecular polarizations contribute cooperatively to the intensity of the band at ~200 cm^{-1} (6 THz). It is also shown that the intensity of the band at ~700 cm^{-1} is reduced by the libration−polarization cross term, in accord with the reduced magnitude of dynamical dipole. The dependence of the calculated spectral profiles on the temperature and potential model is also discussed.

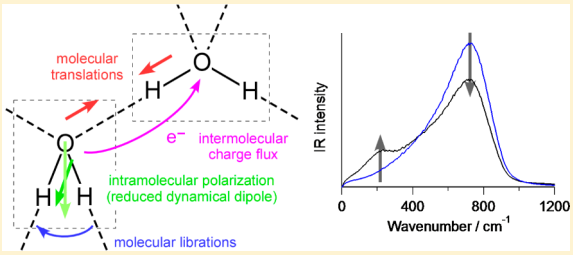

1. INTRODUCTION

There are a few characteristic bands known for the infrared (IR) and Raman spectra of liquid water,[1,2] and their properties have been extensively studied for decades. Because it is a hydrogen-bonding liquid, each of those bands responds rather strongly to various changes in thermodynamic conditions, chemical situations, and so forth. To fully utilize the information contained in those spectral responses to deepen our understanding on what is going on in the liquid, it is required to elucidate detailed mechanisms that determine the spectral features, such as the frequency shifts, intensities, and band widths.

Here, particular attention is paid to the IR and far-IR (terahertz) spectrum in the frequency region below 1000 cm^{-1}. It is characterized by two main bands;[2,3] one is located at ~700 cm^{-1} and arises mainly from molecular librations, while the other is located at ~200 cm^{-1} (6 THz) and arises mainly from O...H hydrogen-bond stretching, or with regard to the molecular degrees of freedom, from molecular translations. It has been pointed out[4−6] that the latter is not sufficiently well reproduced by the use of ordinary classical molecular dynamics (MD) methods, even if the effects of intramolecular polarizations induced by intermolecular electrostatic (such as dipole−induced dipole) interactions[5−9] are taken into account, while it is reasonably reproduced by the use of ab initio MD (AIMD),[4,10−12] suggesting that some behavior of electrons (not included in ordinary classical MD) plays an essential role in the IR intensity generation. With a view to application to large systems, such as aqueous solutions of biomolecules,[13,14] it is desirable to deepen our understanding of the IR intensity generation mechanism and devise a way to incorporate it into classical MD because AIMD simulations are computationally demanding and cannot be carried out for large systems with the computational resources presently available.

In our previous study,[15] by analyzing electron density derivatives (derivatives of electron density by molecular translations), it was shown that fluxes of electrons are induced between molecules (thus called *intermolecular charge fluxes*[16]) by translations of hydrogen-bonded water molecules, and their amplitudes are sufficiently large to give rise to dipole derivatives of 1.5−1.9 D $Å^{-1}$ (average diagonal values).[15,17] It was also shown that, through these dipole derivatives that appear in the expansion of the time derivative of system's dipole, it is possible to incorporate the effects of those intermolecular charge fluxes into spectral simulations based on classical MD[15,18] so that the presence (with significant intensity) of the ~200 cm^{-1} band is reasonably reproduced.

With this simulation method, however, the effects of hydrogen-bond fluctuations and defects on the intermolecular charge fluxes are not taken into account because a common set of dipole derivative parameters is used for all the molecules in the liquid. In fact, as shown in ref 17, the dipole derivatives of the translations of molecules with hydrogen-bond defects have significantly large off-diagonal terms even after taking averages over molecules. This is reasonably understood by considering that the charge fluxes are induced along hydrogen bonds even if their directions are not coincident with those of the molecular translations. It is therefore important to devise a method to incorporate the effects of hydrogen-bond fluctuations and

Received: December 30, 2013
Published: February 18, 2014

dx.doi.org/10.1021/ct4011147 | *J. Chem. Theory Comput.* 2014, 10, 1219−1227

defects into the intensity generation mechanisms used in spectral simulations. Here, one should have in mind that the hydrogen-bond conditions of individual molecules in liquid are dynamically changing so that it is necessary to derive a continuous relation between the properties of charge flux and hydrogen bonding. The method is also required to be friendly with the use of periodic boundary conditions in MD simulations, where molecules repeatedly disappear on one side of the simulation cell and appear on the other.

The purpose of the present study is three-fold. One is to elucidate how the electrons of hydrogen-bonded water molecules are modulated by molecular translations from calculations on water clusters. Instead of analyzing the electron density derivatives,[15] here we have analyzed the derivatives of the electron populations of orbitals (called *electron population derivatives*) and have examined the relation between them (especially those related to intermolecular charge fluxes) and the hydrogen-bond conditions of individual molecules. The second is to devise a method, by referring to the relation derived above, of spectral simulations that can incorporate the effects of hydrogen-bond fluctuations and defects into the spectral intensity generation. Here, we have also taken into account the effects of intramolecular polarizations induced by intermolecular electrostatic interactions in the spectral intensity generation and have examined how the three intensity generation mechanisms (molecular libration, intermolecular charge flux, and intramolecular polarization) work cooperatively to determine the spectral profiles. The third is to examine how well the spectral simulation method thus devised can reproduce the temperature dependence of the spectral profiles. The origin of the dependence of the calculated spectral profiles on the potential models used in MD will also be discussed.

2. COMPUTATIONAL PROCEDURE

2.1. Analysis of Electron Population Derivatives for Water Clusters. The modulations in the electron population induced by molecular translations along hydrogen bonds are represented as the electron population derivatives $\partial\rho_{r[m]}/\partial X_{\alpha[n]}$, where $\rho_{r[m]}$ is the population of orbital r of molecule m, and $X_{\alpha[n]}$ stands for the translation motion of molecule n along hydrogen bond α, and were analyzed for the tetrahedrally hydrogen-bonded molecules (i.e., the molecules of double-donor and double-acceptor type) in $(\text{water})_{28}$ and $(\text{water})_{30}$ clusters. As in our previous studies,[15,19] the initial structures of the clusters were taken from the study by Lenz and Ojamäe,[20] and the structures were optimized at the B3LYP/6-31+G (2df,p) level by using the Gaussian 03 program.[21] There are eight tetrahedrally hydrogen-bonded molecules in each cluster. The electron populations $\rho_{r[m]}$ were calculated by the Mulliken population analysis[22] for the equilibrium ($X_{\alpha[n]} = 0$) and displaced ($X_{\alpha[n]} = 0.03$ Å) structures to derive $\partial\rho_{r[m]}/\partial X_{\alpha[n]}$ by numerical differentiation. As clarified in our previous study,[23] the bare Mulliken charges tend to give the wrong sign of intermolecular charge transfer along hydrogen bonds because of the basis set superposition error. Therefore, the effect of the hydrogen-bond formation on $\partial\rho_{r[m]}/\partial X_{\alpha[n]}$ was evaluated as $\delta(\partial\rho_{r[m]}/\partial X_{\alpha[n]})$ $[\equiv(\partial\rho_{r[m]}/\partial X_{\alpha[n]})_{\text{whole\_cluster}} - (\partial\rho_{r[m]}/\partial X_{\alpha[n]})_n - (\partial\rho_{r[m]}/\partial X_{\alpha[n]})_{\text{the\_rest}}]$, where $(\partial\rho_{r[m]}/\partial X_{\alpha[n]})_n$ is the population derivative of molecule n calculated in the sea of ghost atoms of all the other molecules in the cluster, and $(\partial\rho_{r[m]}/\partial X_{\alpha[n]})_{\text{the\_rest}}$ is the population derivative calculated for the translation of ghost atoms of molecule n. The last term is essential for evaluating $\delta(\partial\rho_{r[m]}/\partial X_{\alpha[n]})$, as described in Section 3.1, but it is negligible for the electron density derivatives $[\partial\rho^{(\text{el})}(\boldsymbol{r})/\partial X_{\alpha[n]}]$ that were analyzed in the previous study.[15] For a planar system, there is an efficient way of estimating the changes in atomic partial charges induced by vibrations, which is based on out-of-plane dipole second derivatives.[24−28] However, the present systems are three-dimensional and, hence, incompatible with its use.

For comparison, the electron population derivatives for the OH stretching modes, denoted as $\partial\rho_{r[m]}/\partial Q_{\text{OH}[n]}$, were also calculated. The effect of the hydrogen-bond formation was evaluated by removing the basis set superposition error in a similar way.

2.2. Spectral Simulations. The IR and far-IR spectra were calculated by combining the trajectories of molecules obtained by classical MD and three IR intensity generation mechanisms, that is, molecular librations (rotations of molecular permanent dipoles), intermolecular charge fluxes, and intramolecular polarizations. The classical MD simulations were carried out for the liquid system of 1024 molecules in a cubic cell by using the TIP4P[29] and TIP5P[30] potential models at 298.15 K (for the results in Ssection 3.2) and additionally at other temperatures and also by using the TIP4P/Ew,[31] TIP4P/2005,[32] TIP4P/Ice,[33] TIP3P,[34] and SPC/E[35] potential models (for the results in Section 3.3). The volume of the cubic cell was fixed by referring to the experimental density of liquid water. The time step was set to 1 fs, and the spectra were calculated from the trajectories during 14 ns.

The formula for calculating the spectra $\alpha_{\text{IR}}(\omega)$ is expressed as[5]

$$\alpha_{\text{IR}}(\omega) = \frac{4\pi\omega\tanh(\beta\hbar\omega/2)}{3\hbar n(\omega)cV} \times \int_{-\infty}^{\infty} \mathrm{d}t\, \exp(i\omega t)\langle \boldsymbol{M}(t)\cdot\boldsymbol{M}(0)\rangle \tag{1}$$

where $\boldsymbol{M}(t)$ is the total dipole moment of the system at time t, $n(\omega)$ is the frequency-dependent refractive index (but the frequency dependence was neglected in the present study), V is the volume of the system, and $\beta = 1/k_{\text{B}}T$ at temperature T. The duration of the integration for the Fourier transform in eq 1 was set to 65.5 ps to secure the frequency resolution of 0.5 cm^{-1}. The IR intensity generation mechanisms are related to how $\boldsymbol{M}(t)$ is evaluated. The simplest one is the sum of the molecular dipole moments derived from the fixed partial charges used in the potential models and constitutes the main factor of the IR intensity of the band at ∼700 cm^{-1} (known as arising from molecular librations). The dipole moments arising from the other two intensity generation mechanisms were treated as follows.

As described in Section 3.1, the analysis of $\partial\rho_{r[m]}/\partial X_{\alpha[n]}$ indicates that the derivative of the extent of intermolecular transfer of electron population through a hydrogen bond is represented as approximately linear to the length of the hydrogen bond. This linear relation is expressed as

$$\frac{\partial\rho_{\text{D}\leftarrow\text{A}}}{\partial r_{\text{O...H}}} = -b_{\text{icf}}(r_{\text{O...H}} - r_{\text{thrsh}}) \qquad (r_{\text{O...H}} \le r_{\text{thrsh}}) \tag{2}$$

where $\rho_{\text{D}\leftarrow\text{A}}$ is the extent of transfer of electron population from hydrogen-bond acceptor to donor (the molecular total value, as explained in Section 3.1), $r_{\text{O...H}}$ is the hydrogen-bond length, and $-b_{\text{icf}}$ and $b_{\text{icf}}\, r_{\text{thrsh}}$ are the coefficients of this linear relation obtained from the plot of $\rho_{\text{D}\leftarrow\text{A}}$ against $r_{\text{O...H}}$ (shown in Section 3.1). As implied, r_{thrsh} has the meaning of the threshold

hydrogen-bond length of the electron population transfer. Therefore, by integrating $\partial\rho_{D\leftarrow A}/\partial r_{O\cdots H}$ from r_{thrsh} to a shorter bond length, the value of $\rho_{D\leftarrow A}$ is calculated as

$$\rho_{D\leftarrow A} = \frac{b_{icf}}{2}(r_{O\cdots H} - r_{thrsh})^2 \qquad (r_{O\cdots H} \le r_{thrsh}) \tag{3}$$

As a result, the dipole moment arising from the intermolecular charge fluxes was calculated as the sum of the bond dipoles of the hydrogen bonds, evaluated by placing the electric charges derived from eq 3 on the oxygen atoms of the hydrogen-bonded molecules. Because the electric charges derived from eq 3 (by using the values of b_{icf} and r_{thrsh} obtained in Section 3.1) are small (e.g., ~0.01 e for $r_{O\cdots H}$ = 1.9 Å) and many molecules in the liquid donate and accept two hydrogen bonds, we assume that the effect of this term on the potential functions for MD is negligible. However, because the electric charges are modulated and are transferred over long distances (between molecules) by the changes in $r_{O\cdots H}$, this term gives rise to sufficiently large dipole derivatives, as described in Sections 3.1 and 3.2. The assumption (or approximation) underlying the use of eq 3 is that the intermolecular charge flux through each hydrogen bond is determined independently (in explicit terms) of the situations of the other neighboring hydrogen bonds, and the effect of hydrogen-bond cooperativity on the values of b_{icf} and r_{thrsh} is sufficiently small. In fact, $r_{O\cdots H}$ appearing in eq 3 is intimately related to the hydrogen-bond strength (a shorter $r_{O\cdots H}$ for a stronger hydrogen bond); so the existence of the cooperative effect of the hydrogen-bond strength (affecting the frequency of the intramolecular OH stretching mode[36,37]) does not necessarily mean that there is a similar effect on the values of b_{icf} and r_{thrsh}.

The dipole moment arising from the intramolecular polarizations induced by intermolecular electrostatic interactions was evaluated by placing the molecular polarizability tensor [of 1.16 Å^3, assumed isotropic, obtained at B3LYP/6-31+G(2df,p)] at the molecular center of mass of each molecule and by calculating the electric field from the atomic partial charges (used in the potential functions) of the surrounding molecules. No iterative evaluation procedure was adopted in the present study.

The calculations described above were carried out with our original programs on Dell PowerEdge T610 (with Intel Xeon X5650) and other servers in our laboratory. The computation time needed to calculate each spectrum was equivalent to about 1040 h (in the case of the TIP5P potential model) of a single CPU core of X5650.

3. RESULTS AND DISCUSSION

3.1. Dependence of Intermolecular Charge Fluxes on Hydrogen-Bond Length. The electron population derivatives $\delta(\partial\rho_{r[m]}/\partial X_{\alpha[n]})$, which are defined in the middle of Section 2.1, with the labeling of molecules (m and n) and the directions of molecular translations ($X_{\alpha[n]}$) defined in Figure 1, are shown in Table 1. The values for the valence s and p orbitals are shown for the oxygen atoms of molecules **1** and **2**, while only the total values are shown for the other atoms and molecules. Because both translations of molecules **1** and **2** result in a change in the length of the hydrogen bond between them, the two sets of electron population derivatives should be considered as a pair. Noting that each of these molecules is hydrogen bonded also to other three molecules and the values of $\delta(\partial\rho_{r[n]}/\partial X_{\alpha[n]})$ (i.e., of the moving molecule) are directly affected also by those

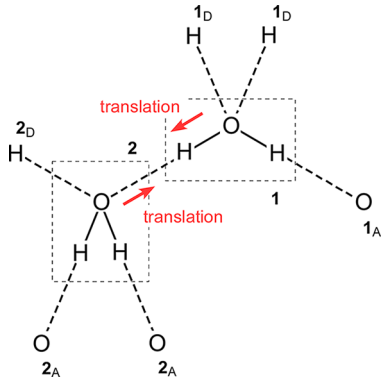

Figure 1. Labeling of molecules and directions of molecular translations used for calculating electron population derivatives.

hydrogen bonds, we regard the values of $\delta(\partial\rho_{r[2]}/\partial X_{\alpha[1]})$ and $\delta(\partial\rho_{r[1]}/\partial X_{\alpha[2]})$ (for $X_{\alpha[1]}$ and $X_{\alpha[2]}$ depicted in Figure 1) as approximately representing the genuine effect of the change in the length of the hydrogen bond between **1** and **2**. Indeed, the molecular total values of these derivatives (-9.61×10^{-2} and 10.39×10^{-2} Å^{-1} shown in Table 1) are sufficiently close to each other in absolute values.

As explained in Section 2.1, in evaluating $\delta(\partial\rho_{r[m]}/\partial X_{\alpha[n]})$, it is essential to remove the basis set superposition error as $\delta(\partial\rho_{r[m]}/\partial X_{\alpha[n]}) = (\partial\rho_{r[m]}/\partial X_{\alpha[n]})_{whole\_cluster} - (\partial\rho_{r[m]}/\partial X_{\alpha[n]})_n - (\partial\rho_{r[m]}/\partial X_{\alpha[n]})_{the\_rest}$. For example, for the molecular total values of $\delta(\partial\rho_{r[2]}/\partial X_{\alpha[1]})$ and $\delta(\partial\rho_{r[1]}/\partial X_{\alpha[2]})$, the first term $[(\partial\rho_{r[m]}/\partial X_{\alpha[n]})_{whole\_cluster}]$ is calculated as 2.23×10^{-2} and 0.24×10^{-2} Å^{-1}. By adding the second term $[-(\partial\rho_{r[m]}/\partial X_{\alpha[n]})_n]$, we have -1.82×10^{-2} and 7.44×10^{-2} Å^{-1}. The last term $[-(\partial\rho_{r[m]}/\partial X_{\alpha[n]})_{the\_rest}$, arising from the translation of ghost atoms of molecule n] is also important, and by adding this also, we obtain -9.61×10^{-2} and 10.39×10^{-2} Å^{-1}, which are the values shown in Table 1.

By inspecting the values shown in Table 1, it is noticed that the gain and loss of electron populations of molecules **1** and **2** are not distributed uniformly among the orbitals in each molecule. Specifically, large negative values (-4.69×10^{-2} and -5.19×10^{-2} Å^{-1}) are calculated for the s and p_y orbitals but a small positive value (1.56×10^{-2} Å^{-1}) is calculated for the p_x orbital of the oxygen atom of **2** for the translation of **1**, and large positive values (5.06×10^{-2} and 3.54×10^{-2} Å^{-1}) are calculated for the p_x and p_z orbitals of the oxygen atom of **1** for the translation of **2**. The tendency that the p_y orbital is likely to lose electrons upon strengthening of an accepting hydrogen bond, while the p_x and p_z orbitals are likely to gain electrons upon strengthening of a donating hydrogen bond, is consistent with the observed difference in the electron populations between the gas-phase molecule and ice.[38] However, according to this experiment, the population of the 2s orbital of the oxygen atom is larger in ice than in the gas-phase molecule;[38] so this does not explain the large negative value calculated for the s orbital of the oxygen atom of **2** upon translation of **1**. For comparison, the electron population derivatives for the OH stretching mode of **1** are also shown in Table 1. It is clearly seen that the gain and loss of electron populations of molecules **1** and **2** are nonuniform among the orbitals in each molecule also in this case, and the positive/negative pattern of the values is quite similar to that seen for the molecular translations.

The electron population derivatives shown in Table 1 are average values; those calculated for each $X_{\alpha[n]}$ (four directions

dx.doi.org/10.1021/ct4011147 | J. Chem. Theory Comput. 2014, 10, 1219−1227

Table 1. Electron Population Derivatives Calculated for Molecular Translations and OH Stretches of Tetrahedrally Hydrogen-Bonded Water Molecules in $(water)_{28}$ and $(water)_{30}$ Clusters[a,b]

molecule	atom	orbital[c]	electron population derivative (10^{-2} Å^{-1}) translation of **1**	translation of **2**	OH stretch of **1**[d]
1	total		13.09	10.39	22.43
	O	total	12.29	10.03	36.59
		s	1.31	0.53	3.05
		p_x	2.53	5.06	15.84
		p_y	5.75	0.10	−2.08
		p_z	2.49	3.54	18.00
	H (H-bonded to **2**)	total	−0.95	−0.67	−15.43
	H (other)	total	1.75	1.04	1.27
2	total		−9.61	−13.70	−20.55
	O	total	−9.32	−11.99	−17.23
		s	−4.69	−3.53	−5.33
		p_x	1.56	−0.30	4.41
		p_y	−5.19	−7.57	−13.51
		p_z	−1.33	−0.64	−2.60
	H	total (each atom)	−0.16	−0.85	−1.66
$\mathbf{1}_A$	total		3.08		
$\mathbf{1}_D$	total (each molecule)		−3.10		
$\mathbf{2}_A$	total (each molecule)			2.19	
$\mathbf{2}_D$	total			−1.29	

[a]Average values calculated at the B3LYP/6-31+G(2df,p) level. See Figure 1 for the labeling of the molecules and the directions of molecular translations. [b]See text in Section 2.1 for the method of avoiding the basis set superposition error and extracting the effect of hydrogen-bond formation. [c]Molecular axes (*z* along the HOH bisection, *x* along the other in-plane direction, and *y* along the out-of-plane direction) of each molecule are used. [d]Stretch of the OH bond involved in the hydrogen bond between **1** and **2** (i.e., the OH bond on the left-hand side of **1** depicted in Figure 1), in units of 10^{-2} Å^{-1} amu$^{-1/2}$.

for each of 16 molecules examined here) are distributed around them. Then, one may ask how each of those distributed values is related to the dipole derivative $\partial\boldsymbol{\mu}/\partial X_{\alpha[n]}$. In fact, the latter is reasonably well reproduced by placing the molecular total values of $\delta(\partial\rho_{r[m]}/\partial X_{\alpha[n]})$ (obtained by taking the sum over *r*) on the oxygen atoms of all molecules *m*, as shown in Figure 2(a), or even by using those of only the moving molecule (*n*) and its four hydrogen-bonded molecules, as shown in Figure 2(b). It may be said, therefore, that the variations in the values of $\delta(\partial\rho_{r[m]}/\partial X_{\alpha[n]})$ rather correctly reflect the effects of different hydrogen-bond conditions of molecules on the extent of intermolecular transfer of electrons.

As stated above, we regard the values of $\delta(\partial\rho_{r[2]}/\partial X_{\alpha[1]})$ and $\delta(\partial\rho_{r[1]}/\partial X_{\alpha[2]})$ (for $X_{\alpha[1]}$ and $X_{\alpha[2]}$ depicted by arrows in Figure 1) as approximately representing the genuine effect of the change in the length of the hydrogen bond between **1** and **2**. Therefore, the molecular total values of $-\delta(\partial\rho_{r[2]}/\partial X_{\alpha[1]})$ and $\delta(\partial\rho_{r[1]}/\partial X_{\alpha[2]})$ are considered to be reasonable estimates of $\partial\rho_{D\leftarrow A}/\partial r_{O\cdots H}$. They are plotted against the hydrogen-bond lengths $r_{O\cdots H}$ in Figure 3(a). It is recognized that the two quantities are in an approximate linear relation (eq 2), with the correlation coefficient of −0.89. From linear regression of the plot, shown with a black broken line in Figure 3(a), the coefficients of this linear relation are obtained as b_{icf} = 0.1768 Å^{-2} and r_{thrsh} = 2.374 Å. For comparison, the plot of the dipole derivatives $|\partial\boldsymbol{\mu}/\partial X_{\alpha[n]}|$ against $r_{O\cdots H}$ is shown in Figure 3(b). It is clearly seen that the correlation between these two quantities is worse (with the correlation coefficient of −0.57) than that between $\partial\rho_{D\leftarrow A}/\partial r_{O\cdots H}$ and $r_{O\cdots H}$ shown in Figure 3(a), suggesting that it is most reasonable to use $\partial\rho_{D\leftarrow A}/\partial r_{O\cdots H}$ as a quantity that correlates the variations in hydrogen-bond conditions to those in the intermolecular charge fluxes in the spectral simulations.

It should also be noted, however, that Mulliken population analysis tends to somewhat overestimate the extent of the intermolecular charge transfer upon hydrogen-bond formation even after removing the basis set superposition error. Indeed, the results shown in Figure 2 suggest that the dipole derivatives $|\partial\boldsymbol{\mu}/\partial X_{\alpha[n]}|$ originate mainly from intermolecular charge fluxes, but in fact, there should also be some effects of intramolecular polarizations. According to our recent analysis on the $(water)_{35}$ cluster of C_5 symmetry,[23] the extent of intermolecular charge transfer upon hydrogen-bond formation is overestimated by a factor of about 2 by Mulliken population analysis (shown in Table 2 of ref 23). Therefore, the value of b_{icf} is reduced by this factor (so that b_{icf} = 0.0884 Å^{-2}) in the spectral simulations described below. Indeed, by using this reduced value of b_{icf}, $\rho_{D\leftarrow A}$ is calculated as ∼0.01 *e* for $r_{O\cdots H}$ = 1.9 Å according to eq 3, in reasonable agreement with the result obtained from the electron density analysis in our previous study[23] and also with those obtained in some other previous studies.[39−42]

3.2. Spectral Simulations at 298 K with Component Analysis. The spectra calculated by using the TIP4P and TIP5P potential models for the MD simulations at 298.15 K are shown with black solid lines in Figure 4(a) and (d), respectively. It is clearly seen that the bands at ∼700 (or ∼800) and at ∼200 cm^{-1} are reasonably reproduced, indicating that the intensity generation mechanisms are properly included in the present calculations. The spectra are decomposed into the contributions of molecular libration (blue solid lines), intramolecular polarization(green solid lines), and libration−polarization cross term (light blue broken lines), as well as the sum of the intermolecular charge flux term and the related cross terms (pink dotted-dashed lines). Without the last one, the band at ∼200 cm^{-1} is not properly reproduced, as shown with black dotted-dashed lines, indicating that the intermolecular

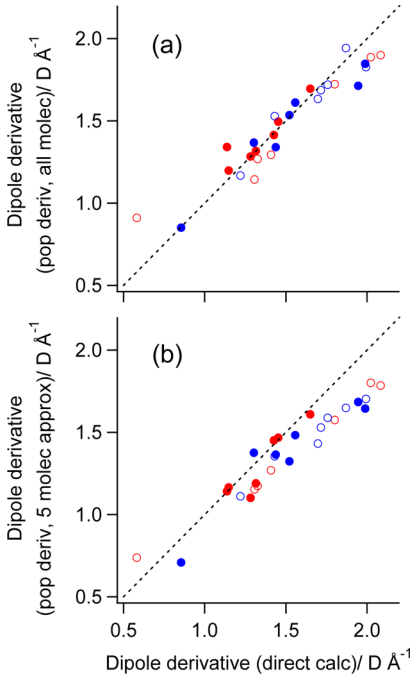

Figure 2. (a) Dipole derivatives $|\partial\boldsymbol{\mu}/\partial X_{\alpha[n]}|$ estimated by placing the molecular total values of $\delta(\partial\rho_{r[m]}/\partial X_{\alpha[n]})$ on the oxygen atoms of all molecules (m) and (b) those estimated by using the molecular total values of $\delta(\partial\rho_{r[m]}/\partial X_{\alpha[n]})$ of only the moving molecule (n) and its four hydrogen-bonded molecules plotted against the directly calculated values of $|\partial\boldsymbol{\mu}/\partial X_{\alpha[n]}|$ of the tetrahedrally hydrogen-bonded molecules in $(water)_{28}$ and $(water)_{30}$ clusters (red and blue markers, respectively). Those obtained for the translations of hydrogen-bond donating and accepting molecules (molecules **1** and **2**, Figure 1) are shown with open and filled circles, respectively. The black broken line is drawn with the gradient of unity through the origin for the guide to the eye.

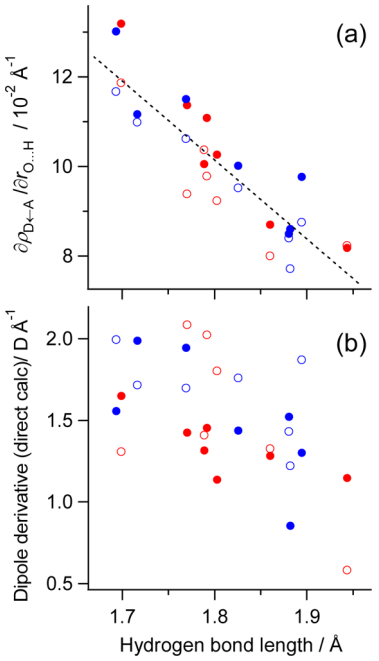

Figure 3. (a) Values of $\partial\rho_{D\leftarrow A}/\partial r_{O\cdots H}$ [estimated as $-\delta(\partial\rho_{r[2]}/\partial X_{\alpha[1]})$ and $\delta(\partial\rho_{r[1]}/\partial X_{\alpha[2]})$, see text in Section 3.1], and (b) dipole derivatives $|\partial\boldsymbol{\mu}/\partial X_{\alpha[1]}|$ and $|\partial\boldsymbol{\mu}/\partial X_{\alpha[2]}|$ (the same quantities as those plotted on the abscissa in Figure 2) plotted against the hydrogen-bond length between molecules **1** and **2** of $(water)_{28}$ and $(water)_{30}$ clusters (red and blue markers, respectively). Those obtained for $X_{\alpha[1]}$ and $X_{\alpha[2]}$ (depicted by arrows in Figure 1) are shown with open and filled circles, respectively. The black broken line in part a, with b_{icf} = 0.1768 Å^{-2} and r_{thrsh} = 2.374 Å in eq 2, is obtained by least-squares fitting.

charge flux plays an essential role in generating the intensity of this band. It is also noticed that the intensity of the ~700 cm^{-1} band is significantly reduced by the libration−polarization cross term, in accord with the result obtained in our previous study[23] that the dynamical dipole (the change in the dipole moment upon molecular rotation[43]) is reduced by intermolecular interactions.

Inspecting the contributions of the intermolecular charge flux (red solid lines) and the related cross terms (purple and light green broken lines) shown in Figure 4(b) and (e) [expanded and detailed views of the spectra shown in Figure 4(a) and(d)], it is noticed that the two cross terms are essential in the intensity generation of the ~200 cm^{-1} band. That is, both of these cross terms are larger than the intermolecular charge flux term itself and contribute constructively to give rise to the intensity of the ~200 cm^{-1} band. Therefore, it may be said that in addition to the molecular libration term, which arises from simple rotations of molecular dipole, the intermolecular charge flux and the intramolecular polarization contribute cooperatively in determining the far-IR spectral intensities of liquid water.

Comparing with the spectra calculated in our previous study,[15] on the basis of the dipole derivative parameters that are common to all the molecules, which are shown in Figure 4(c) and(f), it is recognized that the spectral profiles are somewhat different between the two simulation methods. Especially in the case of TIP4P, the role of the intermolecular charge flux−libration cross term is different; it contributes constructively to the intensity at ~200 cm^{-1} in the present calculation but destructively in the previous calculation. These results are considered to indicate that the effects of hydrogen-bond fluctuations and defects (included only in the present calculation) are important in determining the detailed spectral profiles in the far-IR region.

3.3. Dependence on Temperature and Potential Model. The spectra calculated by using the TIP4P, TIP4P/Ew, TIP4P/2005, TIP4P/Ice, TIP3P, TIP5P, and SPC/E potential models for the MD simulations at 273.15, 298.15, 323.15, and 348.15 K are shown in Figure 5. Comparing the spectra calculated at different temperatures with each potential model, it is seen that as the temperature increases, the band at ~200 cm^{-1} becomes less distinct, and the band at ~700 (or ~800) cm^{-1} shifts to the lower-frequency side, in accord with the observed temperature dependence of the spectra shown in ref 3. By performing a component analysis for each of these calculated spectra in the same way as shown in Section 3.2, it is recognized that the reduced clarity of the ~200 cm^{-1} band at higher temperatures seen in Figure 5 arises mainly from the low-frequency shift and the broadening to the low-frequency side of the molecular libration band (including the libration−polarization cross term). In fact, the sum of the intermolecular charge flux term and the related cross terms becomes somewhat reduced in intensity (with a slight low-frequency shift) at ~200 cm^{-1} upon increasing temperature, but it turns out that its effect is minor. As anticipated, the low-frequency shift of the molecular libration modes is due to the weakening of the intermolecular hydrogen bonds (so that the molecules become less constrained by hydrogen bonds). It may be said, therefore,

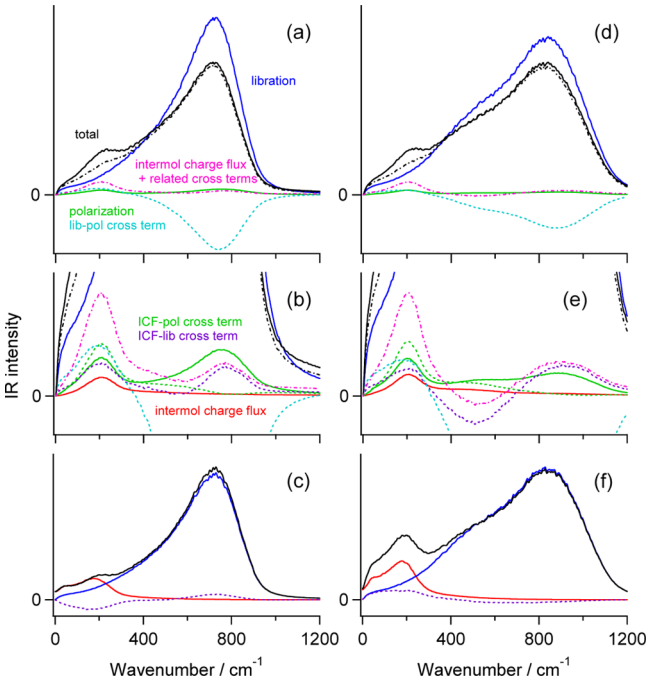

Figure 4. Infrared and far-infrared spectrum in the 0−1200 cm^{-1} region (black solid line) and the contributions of individual mechanisms of intensity generation (color lines) calculated for liquid water at 298.15 K using the (a−c) TIP4P and (d−f) TIP5P potential models for MD. (a and d) Spectrum calculated with the method described in Section 2.2. Blue solid line: molecular libration. Green solid line: intramolecular polarization. Light blue broken line: libration−polarization cross term. Black dotted-dashed line: sum of these three. Pink dotted-dashed line: sum of the intermolecular charge flux term and the related cross terms. (b and e) The same spectrum as in part a and d but drawn with the ordinate scale expanded by a factor of 8. Red solid line: intermolecular charge flux (ICF). Purple broken line: ICF−libration cross term. Light green broken line: ICF−polarization cross term. (c and f) Spectrum calculated with the method described in ref 15. Intramolecular polarization is not explicitly taken into account in this case.

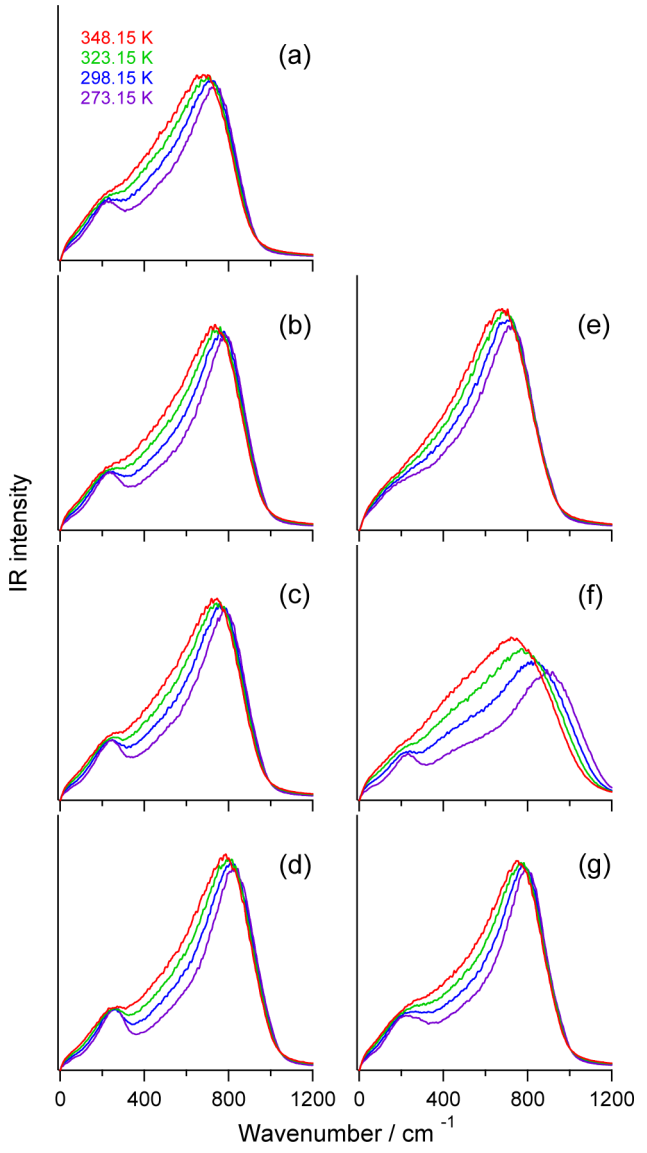

Figure 5. Infrared and far-infrared spectra in the 0−1200 cm^{-1} region of liquid water calculated at 273.15, 298.15, 323.15, and 348.15 K (drawn with purple, blue, green, and red lines, respectively) with the (a) TIP4P, (b) TIP4P/Ew, (c) TIP4P/2005, (d) TIP4P/Ice, (e) TIP3P, (f) TIP5P, and (g) SPC/E potential models used for MD.

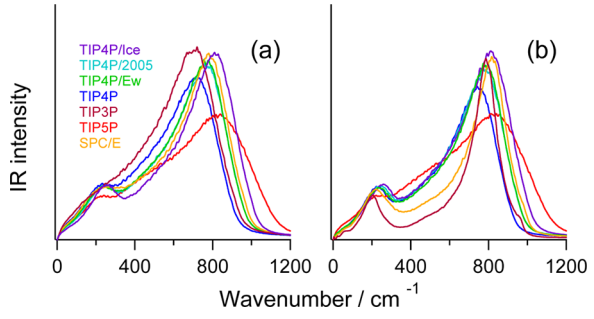

Figure 6. Infrared and far-infrared spectra in the 0−1200 cm^{-1} region of liquid water calculated with the TIP4P, TIP4P/Ew, TIP4P/2005, TIP4P/Ice, TIP3P, TIP5P, and SPC/E potential models used for MD at (a) 298.15 K and (b) the melting point + 25 K. The melting point for each potential model is taken from refs 32, 33, and 47.

that the changes in the spectral profiles seen upon increasing the temperature are regarded as mainly arising from a partial merger of the bands at ∼200 and ∼700 cm^{-1} due to the weakening of the intermolecular hydrogen bonds.

It is also seen in Figure 5 that the calculated spectral profiles vary significantly with the potential models used in the calculations. For ease of comparison, the spectra calculated at 298.15 K are overlapped in Figure 6(a). Among the four TIP4P-type potential models, the band at ∼200 cm^{-1} is most distinct for TIP4P/Ice, least distinct for TIP4P, and intermediate for TIP4P/Ew and TIP4P/2005 (close to each other). Similarly to the temperature dependence of the spectra discussed above, this change occurs in parallel to the frequency shift of the molecular libration band at ∼700 (or ∼800) cm^{-1}. With regard to the other three potential models, the band at ∼200 cm^{-1} is not clearly recognizable for TIP3P, the molecular libration band is the broadest (especially to the high-frequency side) for TIP5P, while the use of SPC/E results in a spectrum that is close to those calculated with TIP4P/Ew and TIP4P/2005.

Considering that the molecular libration band is excessively broad only for TIP5P, it is expected that this feature is related to the presence of the negative point charges that are used for

dx.doi.org/10.1021/ct4011147 | J. Chem. Theory Comput. 2014, 10, 1219−1227

representing the oxygen lone pairs in TIP5P. To support this discussion, the spectra of molecular librations of individual molecules at short time intervals are calculated for TIP5P and (for comparison) TIP4P by substituting the *molecular* dipoles[44] arising only from fixed partial charges for $\boldsymbol{M}$ in eq 1 and by taking the Fourier transforms during the time interval as short as 1 ps. Then, the relation between the intensity-weighted average frequency and the H...L(M) distance of the hydrogen bond (the average value taken for those donated by the librating molecule during the time interval of 1 ps) is examined, where L and M denote the negative point charge(s) used in TIP5P and TIP4P. The result is shown in Figure 7. It is seen

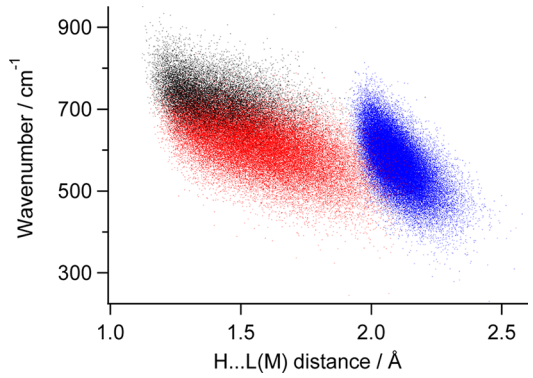

Figure 7. Relation between the intensity-weighted average frequency of the IR spectrum of molecular libration of each individual molecule during a time interval of 1 ps and the H...L(M) distance of the hydrogen bond (the average value taken for those donated by the librating molecule) calculated with the TIP5P (red and black dots) and TIP4P (blue dots) potential models, where L and M denote the negative point charge(s) used in TIP5P and TIP4P. For TIP5P, the molecules with spectral intensity larger than 25% in the frequency region higher than 900 cm^{-1} are shown with black dots and the others with red dots.

that for both TIP5P (red and black dots) and TIP4P (blue dots), the molecular libration band tends to be located at a higher frequency position for a molecule with a short H...L(M) distance of the donating hydrogen bond. In the case of TIP5P, the molecules with significant spectral intensity (larger than 25%) in the frequency region higher than 900 cm^{-1} are shown with black dots. About 79% of those molecules have H...L distances shorter than 1.5 Å, while only about 46% among all the molecules have such short H...L distances, indicating that the molecules with short H...L distances are mainly responsible for the spectral broadening to the high-frequency side seen for TIP5P.

It has recently been suggested that differences in the structural, dynamical, and spectroscopic properties of liquid water obtained with various computational models are partly due to the difference in the calculated melting point, so that the "relative-to-melting" temperature scale is useful for discussing the temperature dependence of those properties.[45,46] On the basis of this idea, the spectra calculated at the melting point[32,33,47] + 25 K with the seven potential models are shown in Figure 6(b). It is noticed that the spectral profiles calculated with the four TIP4P-type potential models approximately coincide with each other in the 0−750 cm^{-1} region, indicating that the difference among these four spectral profiles seen in this frequency region at 298.15 K [shown in Figure 6(a)] is due to the difference in the melting point. It is also seen in Figure 6(b) that the spectrum calculated with TIP3P has a distinct feature at ∼200 cm^{-1}, indicating that the vagueness of the spectral feature at around this frequency calculated at 298.15 K [shown in Figures 5(e) and 6(a)] is due to the too low melting point of this potential model (145.6 K).[47]

To see how the approximate coincidence of the spectra calculated with the four TIP4P-type potential models at the melting point + 25 K is related to the liquid structures, the radial distribution functions are calculated with these potential models. The result is shown in Figure 8. It is seen that for all

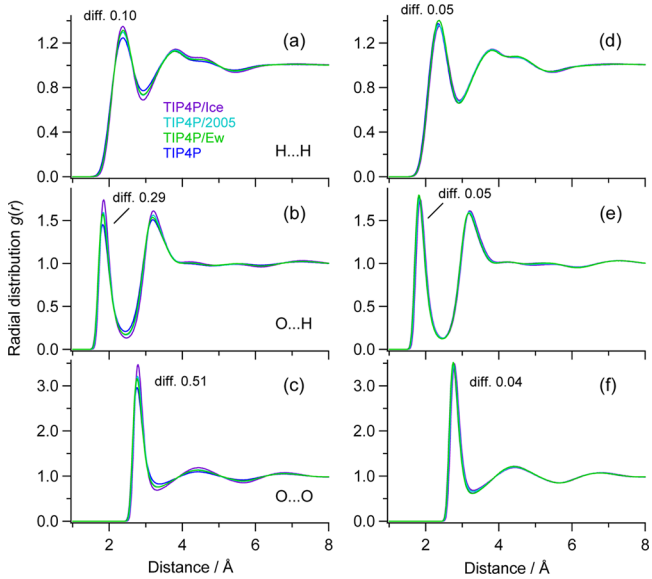

Figure 8. H...H, O...H, and O...O radial distribution functions calculated with the TIP4P (blue), TIP4P/Ew (green), TIP4P/2005 (light blue), and TIP4P/Ice (purple) potential models at (a−c) 298.15 K and (d−f) the melting point + 25 K. Difference in the peak height among the four potential models is shown for each radial distribution function.

the three (H...H, O...H, and O...O) radial distribution functions, the difference in the peak height among the four potential models is smaller at the melting point + 25 K [shown in Figure 8(d−f)] than at 298.15 K [shown in Figure 8(a−c)]. In other words, the approximate coincidence of the spectra seen at the melting point + 25 K is (at least partly) explained by the similarity of the liquid structural features obtained with the use of the relative temperature scale.

4. CONCLUDING REMARKS

Detailed understanding of the intensity generation mechanisms is an important factor in spectral analysis, especially in the cases where the spectrum under study is rather broad and the component bands are not well separable on the frequency axis. In the present study, simulations of the IR and far-IR (terahertz) spectrum of liquid water in the frequency region below 1000 cm^{-1} have been carried out by taking into account three intensity generation mechanisms (which induce modulations of system's dipole $\boldsymbol{M}(t)$ in eq 1): molecular libration, intermolecular charge flux, and intramolecular polarization. The first one is simple; it stands for rotation of molecular permanent dipole. The third one is rather well known from a previous time and is often incorporated in the form of the dipole−induced dipole interaction. In the present study, the intermolecular

dx.doi.org/10.1021/ct4011147 | J. Chem. Theory Comput. 2014, 10, 1219−1227

electric field is not calculated with the dipole approximation but by using the atomic partial charges. Meanwhile, the second one (intermolecular charge flux) is a direct consequence of the intermolecular charge transfer occurring upon hydrogen-bond formation, in which there is increasing interest recently.[15,17,19,23,27,28,39−42,48−52] In the present study, on the basis of population analysis (with the basis set superposition error being avoided) carried out for water clusters, it is shown that there is an approximate linear relation (eq 2) between the derivative of intermolecular electron population transfer ($\partial\rho_{D\leftarrow A}/\partial r_{O\cdots H}$) and the hydrogen-bond length ($r_{O\cdots H}$). The resulting integrated formula (eq 3) is friendly with the use of the periodic boundary condition in MD and has been used in the present spectral simulations to take into account the effects of hydrogen-bond fluctuations and defects. The cooperative contributions of the three intensity generation mechanisms, as well as the dependence of the calculated spectral profiles on temperature and potential model, have been examined.

Hydrogen-bond fluctuations and defects are present not only in neat liquid water but also (perhaps more abundantly) around biomolecules dissolved in aqueous solutions; so the present spectral simulation method will be useful in those cases. However, the formula for $\rho_{D\leftarrow A}$ shown in eq 3 has been obtained for hydrogen bonding between water molecules, and at least the values of the coefficients (b_{icf} and r_{thrsh}) may be different for different types of hydrogen bonds, such as those between peptide and water. This kind of detailed parametrization will be essential for understanding the intensity variations of the IR and far-IR (terahertz) spectra induced in various conditions because the intensities are directly related to the modulations of the system's dipole. If we have sufficient understanding on this, we will be able to proceed to fine-tuning of the potential models used in classical MD, including the effect of intermolecular charge flux on the potential functions (although expected to be small as described in Section 2.2), as well as the effect of the asymmetry of hydrogen-bond conditions of the two OH bonds in each molecule[53] on the intramolecular charge distribution. These points would deserve further studies.

AUTHOR INFORMATION

Corresponding Author

*Telephone and Fax: +81-54-238-4624. E-mail: torii@ed.shizuoka.ac.jp.

Notes

The authors declare no competing financial interest.

ACKNOWLEDGMENTS

This study was supported by a Grant-in-Aid for Scientific Research from the Ministry of Education, Culture, Sports, Science, and Technology and the Japan Society for the Promotion of Science.

REFERENCES

(1) Walrafen, G. E. *J. Chem. Phys.* **1964**, *40*, 3249−3256.
(2) Bertie, J. E.; Lan, Z. *Appl. Spectrosc.* **1996**, *50*, 1047−1057.
(3) Maréchal, Y. *J. Mol. Struct.* **2011**, *1004*, 146−155.
(4) Heyden, M.; Sun, J.; Funkner, S.; Mathias, G.; Forbert, H.; Havenith, M.; Marx, D. *Proc. Natl. Acad. Sci. U.S.A.* **2010**, *107*, 12068−12073.
(5) Guillot, B. *J. Chem. Phys.* **1991**, *95*, 1543−1551.
(6) Paesani, F.; Xantheas, S. S.; Voth, G. A. *J. Phys. Chem. B* **2009**, *113*, 13118−13130.
(7) Madden, P. A.; Impey, R. W. *Chem. Phys. Lett.* **1986**, *123*, 502−506.
(8) Harder, E.; Eaves, J. D.; Tokmakoff, A.; Berne, B. J. *Proc. Natl. Acad. Sci. U.S.A.* **2005**, *102*, 11611−11616.
(9) Fanourgakis, G. S.; Xantheas, S. S. *J. Chem. Phys.* **2008**, *128*, 074506.
(10) Sharma, M.; Resta, R.; Car, R. *Phys. Rev. Lett.* **2005**, *95*, 187401.
(11) Chen, W.; Sharma, M.; Resta, R.; Galli, G.; Car, R. *Phys. Rev. B* **2008**, *77*, 245114.
(12) Wan, Q.; Spanu, L.; Galli, G. A.; Gygi, F. *J. Chem. Theory Comput.* **2013**, *9*, 4124−4130.
(13) Zhang, C.; Durbin, S. M. *J. Phys. Chem. B* **2006**, *110*, 23607−23613.
(14) Heyden, M.; Havenith, M. *Methods* **2010**, *52*, 74−83.
(15) Torii, H. *J. Phys. Chem. B* **2011**, *115*, 6636−6643.
(16) Torii, H. *J. Chem. Phys.* **2010**, *133*, 034504.
(17) Torii, H. *Chem. Phys.* **2013**, *419*, 90−96.
(18) Hamm, P.; Savolainen, J. *J. Chem. Phys.* **2012**, *136*, 094516.
(19) Torii, H. *J. Phys. Chem. B* **2010**, *114*, 13403−13409.
(20) Lenz, A.; Ojamäe, L. *J. Phys. Chem. A* **2006**, *110*, 13388−13393.
(21) Frisch, M. J.; Trucks, G. W.; Schlegel, H. B.; Scuseria, G. E.; Robb, M. A.; Cheeseman, J. R.; Montgomery, J. A., Jr.; Vreven, T.; Kudin, K. N.; Burant, J. C.; Millam, J. M.; Iyengar, S. S.; Tomasi, J.; Barone, V.; Mennucci, B.; Cossi, M.; Scalmani, G.; Rega, N.; Petersson, G. A.; Nakatsuji, H.; Hada, M.; Ehara, M.; Toyota, K.; Fukuda, R.; Hasegawa, J.; Ishida, M.; Nakajima, T.; Honda, Y.; Kitao, O.; Nakai, H.; Klene, M.; Li, X.; Knox, J. E.; Hratchian, H. P.; Cross, J. B.; Bakken, V.; Adamo, C.; Jaramillo, J.; Gomperts, R.; Stratmann, R. E.; Yazyev, O.; Austin, A. J.; Cammi, R.; Pomelli, C.; Ochterski, J. W.; Ayala, P. Y.; Morokuma, K.; Voth, G. A.; Salvador, P.; Dannenberg, J. J.; Zakrzewski, V. G.; Dapprich, S.; Daniels, A. D.; Strain, M. C.; Farkas, O.; Malick, D. K.; Rabuck, A. D.; Raghavachari, K.; Foresman, J. B.; Ortiz, J. V.; Cui, Q.; Baboul, A. G.; Clifford, S.; Cioslowski, J.; Stefanov, B. B.; Liu, G.; Liashenko, A.; Piskorz, P.; Komaromi, I.; Martin, R. L.; Fox, D. J.; Keith, T.; Al-Laham, M. A.; Peng, C. Y.; Nanayakkara, A.; Challacombe, M.; Gill, P. M. W.; Johnson, B.; Chen, W.; Wong, M. W.; Gonzalez, C.; Pople, J. A. *Gaussian 03*, Revision D.01; Gaussian, Inc., Wallingford CT, 2004.
(22) Mulliken, R. S. *J. Chem. Phys.* **1955**, *23*, 1833−1840.
(23) Torii, H. *J. Phys. Chem. A* **2013**, *117*, 2044−2051.
(24) Dinur, U.; Hagler, A. T. *J. Chem. Phys.* **1989**, *91*, 2949−2958.
(25) Dinur, U. *J. Phys. Chem.* **1991**, *95*, 6201−6211.
(26) Galimberti, D.; Milani, A.; Castiglioni, C. *J. Chem. Phys.* **2013**, *138*, 164115.
(27) Galimberti, D.; Milani, A.; Castiglioni, C. *J. Chem. Phys.* **2013**, *139*, 074304.
(28) Torii, H. *J. Mol. Struct.* **2014**, *1056/1057*, 84−96.
(29) Jorgensen, W. L.; Madura, J. D. *Mol. Phys.* **1985**, *56*, 1381−1392.
(30) Mahoney, M. W.; Jorgensen, W. L. *J. Chem. Phys.* **2000**, *112*, 8910−8922.
(31) Horn, H. W.; Swope, W. C.; Pitera, J. W.; Madura, J. D.; Dick, T. J.; Hura, G. L.; Head-Gordon, T. *J. Chem. Phys.* **2004**, *120*, 9665−9678.
(32) Abascal, J. L. F.; Vega, C. *J. Chem. Phys.* **2005**, *123*, 234505.
(33) Abascal, J. L. F.; Sanz, E.; García Fernández, R.; Vega, C. *J. Chem. Phys.* **2005**, *122*, 234511.
(34) Jorgensen, W. L.; Chandrasekhar, J.; Madura, J. D.; Impey, R. W.; Klein, M. L. *J. Chem. Phys.* **1983**, *79*, 926−935.
(35) Berendsen, H. J. C.; Grigera, J. R.; Straatsma, T. P. *J. Phys. Chem.* **1987**, *91*, 6269−6271.
(36) Ohno, K.; Okimura, M.; Akai, N.; Katsumoto, Y. *Phys. Chem. Chem. Phys.* **2005**, *7*, 3005−3014.
(37) Tainter, C. J.; Ni, Y.; Shi, L.; Skinner, J. L. *J. Phys. Chem. Lett.* **2013**, *4*, 12−17.
(38) Nilsson, A.; Ogasawara, H.; Cavalleri, M.; Nordlund, D.; Nyberg, M.; Wernet, Ph.; Pettersson, L. G. M. *J. Chem. Phys.* **2005**, *122*, 154505.

(39) Vácha, R.; Marsalek, O.; Willard, A. P.; Bonthuis, D. J.; Netz, R. R.; Jungwirth, P. *J. Phys. Chem. Lett.* **2012**, *3*, 107−111.
(40) Ben-Amotz, D. *J. Phys. Chem. Lett.* **2011**, *2*, 1216−1222.
(41) Lee, A. J.; Rick, S. W. *J. Chem. Phys.* **2011**, *134*, 184507.
(42) Glendening, E. D. *J. Phys. Chem. A* **2005**, *109*, 11936−11940.
(43) Pasquarello, A.; Resta, R. *Phys. Rev. B* **2003**, *68*, 174302.
(44) This treatment does not include any effects of the interference (cross terms) among the molecular dipoles in the time correlation function in eq 1, but it is inevitable for analyzing the relation between the spectral features and the hydrogen bond properties of individual molecules.
(45) Paesani, F.; Yoo, S.; Bakker, H. J.; Xantheas, S. S. *J. Phys. Chem. Lett.* **2010**, *1*, 2316−2321.
(46) Yoo, S.; Xantheas, S. S. *J. Chem. Phys.* **2011**, *134*, 121105.
(47) Vega, C.; Sanz, E.; Abascal, J. L. F. *J. Chem. Phys.* **2005**, *122*, 114507.
(48) Ufimtsev, I. S.; Luehr, N.; Martinez, T. J. *J. Phys. Chem. Lett.* **2011**, *2*, 1789−1793.
(49) Zhao, Z.; Rogers, D. M.; Beck, T. L. *J. Chem. Phys.* **2010**, *132*, 014502.
(50) Khaliullin, R. Z.; Bell, A. T.; Head-Gordon, M. *Chem.—Eur. J.* **2009**, *15*, 851−855.
(51) Marenich, A. V.; Olson, R. M.; Chamberlin, A. C.; Cramer, C. J.; Truhlar, D. G. *J. Chem. Theory Comput.* **2007**, *3*, 2055−2067.
(52) Dal Peraro, M.; Raugei, S.; Carloni, P.; Klein, M. L. *ChemPhysChem* **2005**, *6*, 1715−1718.
(53) Zhang, C.; Khaliullin, R. Z.; Bovi, D.; Guidoni, L.; Kühne, T. D. *J. Phys. Chem. Lett.* **2013**, *4*, 3245−3250.